Supplementary Information for

High-dimensional orbital angular momentum multiplexing nonlinear holography

Xinyuan Fang[1,2,*], Haocheng Yang[1,*], Wenzhe Yao[1,*], Tianxin Wang[1], Yong Zhang[1,†], Min Gu[2] and Min Xiao[1,3]

[1]National Laboratory of Solid State Microstructures, College of Engineering and Applied Sciences, and School of Physics, Nanjing University, Nanjing 210093, China.

[2]Centre for Artificial-Intelligence Nanophotonics, School of Optical-Electrical and Computer Engineering, University of Shanghai for Science and Technology, Shanghai, 200093, China.

[3]Department of Physics, University of Arkansas, Fayetteville, Arkansas 72707, USA

*These authors contributed equally to this work.

†Corresponding author. E-mail: zhangyong@nju.edu.cn

This PDF file includes:

Supplementary Notes 1 to 7

Supplementary Figures 1 to 10

Supplementary Text

Supplementary Note 1: Calculation of signal-to-noise ratio (SNR)

In OMNH, SNR is defined as $10\log_{10}(I_{\mathrm{Sig}}/I_{\mathrm{Noise}})$, where I_{Sig} and I_{Noise} represent the intensities of the holographic images reconstructed from the desired OAM channel and the other OAM channels, respectively. Without losing generality, we investigate the SNR in the process of wavelength-multiplexed nonlinear holography (WMNH) shown in Fig. 1c.

The image (intensity distribution) of the output FW in the Fourier plane can be expressed as

$$\begin{aligned} I_1 = E_1 * E_1^* &= [\Im\{e^{i\psi_1}\} + \Im\{e^{i\psi_2}\} \otimes \Im\{e^{il_{en}\varphi}\}] * [\Im\{e^{i\psi_1}\} + \Im\{e^{i\psi_2}\} \otimes \Im\{e^{il_{en}\varphi}\}]^* \\ &= \left|\Im\{e^{i\psi_1}\}\right|^2 + \left|\Im\{e^{i\psi_2}\} \otimes \Im\{e^{il_{en}\varphi}\}\right|^2 + [\Im\{e^{i\psi_1}\}] * [\Im\{e^{i\psi_2}\} \otimes \Im\{e^{il_{en}\varphi}\}]^* + [\Im\{e^{i\psi_1}\}]^* * [\Im\{e^{i\psi_2}\} \otimes \Im\{e^{il_{en}\varphi}\}] \end{aligned} \tag{S1}$$

Here, $e^{i\psi_1}$ and $e^{i\psi_2}$ are the Fourier holograms of the patterns N and J, respectively, l_{en} is the order of encoding helical phase on pattern J. And $\otimes$ and $\Im\{\ \}$ denote the operators of convolution and Fourier transformation, respectively. The first term in Eq. (1) corresponds to the signal information to reconstruct the pattern N in FW. Three additional terms can be seen as crosstalk caused by the SHW channel, i.e., the hologram of pattern J. Based on the orthogonality of OAM modes in the spatial frequency domain (SFD), the crosstalk can be effectively filtered out by a mask of hole array (Fig. S5).

By using MATLAB R2016b, the first term $\left|\Im\{e^{i\psi_1}\}\right|^2$ can be directly calculated through fast Fourier transform. It is time-consuming to calculate the convolution in the rest terms directly. Therefore, we perform inverse Fourier transform of, for example, the second term $\left|\Im\{e^{i\psi_2}\} \otimes \Im\{e^{il_{en}\varphi}\}\right|^2$, and calculate $\Im^{-1}\left\{\Im\{e^{i\psi_2}\} \otimes \Im\{e^{il_{en}\varphi}\}\right\}$. The convolution is then simplified to be the multiplication of $e^{i\psi_2}$ and $e^{il_{en}\varphi}$ according to the property of Fourier transform. The third and fourth terms can be calculated likewise.

The hole array is denoted as *Filter*, we have

$$Signal = \left|\Im\{e^{i\psi_1}\}\right|^2 * Filter \tag{S2}$$

$$Noise = \left\{\left|\Im\{e^{i\psi_2}\} \otimes \Im\{e^{il_{en}\varphi}\}\right|^2 + [\Im\{e^{i\psi_1}\}]^* [\Im\{e^{i\psi_2}\} \otimes \Im\{e^{il_{en}\varphi}\}] + [\Im\{e^{i\psi_1}\}][\Im\{e^{i\psi_2}\} \otimes \Im\{e^{il_{en}\varphi}\}]^*\right\} * Filter$$

Then, we obtain $SNR \equiv 10\lg\dfrac{\|Signal\|}{\|Noise\|}$, in which $\|\cdot\|$ means the 2-norm of a matrix.

When a decoding vertically-polarized FW with a spiral phase of l_{de} participates in the type-II SHG, the intensity of the SHW in the Fourier plane can be described as

$$I_2 = (E_2)(E_2)^* = [\Im\{Ce^{i\psi_1}\} \otimes \Im\{e^{il_{de}\varphi}\} + \Im\{Ce^{i\psi_2}\} \otimes \Im\{e^{i(l_{en}+l_{de})\varphi}\}][\Im\{Ce^{i\psi_1}\} \otimes \Im\{e^{il_{de}\varphi}\} + \Im\{Ce^{i\psi_2}\} \otimes \Im\{e^{i(l_{en}+l_{de})\varphi}\}]^* \tag{S3}$$

Here, C is a constant in a given nonlinear process, which is proportional to the nonlinear coefficient $\chi^{(2)}$ of the crystal. When $l_{en}+l_{de}=0$, the useful information in each pixel of the SH images is reconstructed as a Gaussian mode solid spot. Therefore, Eq. (S3) can be rewritten as

$$I_2 = \left|\Im\{Ce^{i\psi_2}\}\right|^2 + \left|\Im\{Ce^{i\psi_1}\} \otimes \Im\{e^{il_{de}\varphi}\}\right|^2 + [\Im\{Ce^{i\psi_2}\}][\Im\{Ce^{i\psi_1}\} \otimes \Im\{e^{il_{de}\varphi}\}]^* + [\Im\{Ce^{i\psi_2}\}][\Im\{Ce^{i\psi_1}\} \otimes \Im\{e^{il_{de}\varphi}\}]^* \tag{S4}$$

Signal information (the first term in Eq. (S4)) can be selected by another hole array. The procedure to calculate the SNR for SHW field is similar to the FW case. The calculated SNRs of FW and SHW vary with the encoding l_{en} as shown in the following figure.

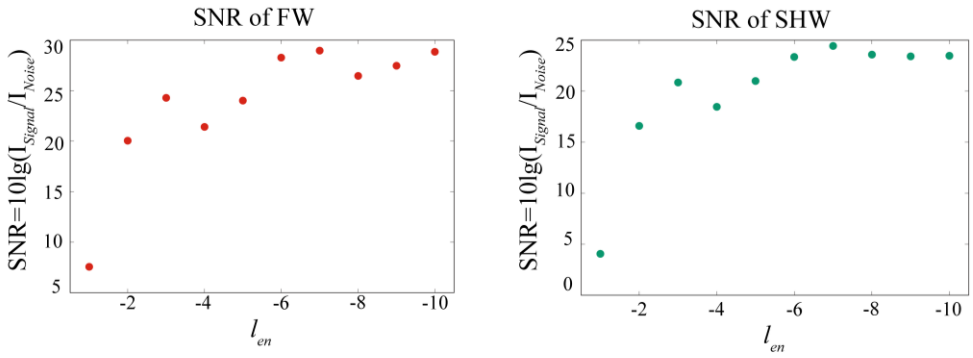

Supplementary Note 2: Calculation of sampling constants at FW (d_ω) and SHW ($d_{2\omega}$)

In a polar coordinate system, the field with a spiral phase can be express as

$$\psi_{SP}(r,\varphi) = circ(\frac{r}{R})\exp(il\varphi) \tag{S5}$$

where l is the topological charge, R defines the size of the field, and r and φ are the radius and azimuthal angle in the polar coordinate, respectively. The modulus amplitude of its spatial frequency can be calculated by

$$\left|E(\rho,\theta)\right| = abs\left|FFT(\psi_{SP})\right| = \left|\frac{(-1)^{l+1}k}{f}\exp(il\theta)\int_0^R J_l(\frac{k}{f}r\rho)rdr\right| \tag{S6}$$

where $k=2\pi/\lambda$ is the wave-number of incident light and f is the focal length of a Fourier lens. r and ρ are the radii in the hologram plane and image plane, respectively. Because the modulus amplitude features a radial symmetry, its distribution along an arbitrary radius direction can be described by

$$\left|E(\rho,0)\right| = \left|\frac{(-1)^{l+1}k}{f}\int_0^R J_l(\frac{k}{f}r\rho)rdr\right| \tag{S7}$$

In our work, we define d_ω (FW)and $d_{2\omega}$ (SH) as the diameters of a circle whose center lies at the light spot center and on whose edge the field modulus amplitude is 30% of the maximal modulus amplitude. We use the experimental parameters for the calculations here (R=4.3mm, f= 75mm). In the figure below, the sampling constants d_ω (FW)and $d_{2\omega}$ (SHW) for l=4 are analysed as an example.

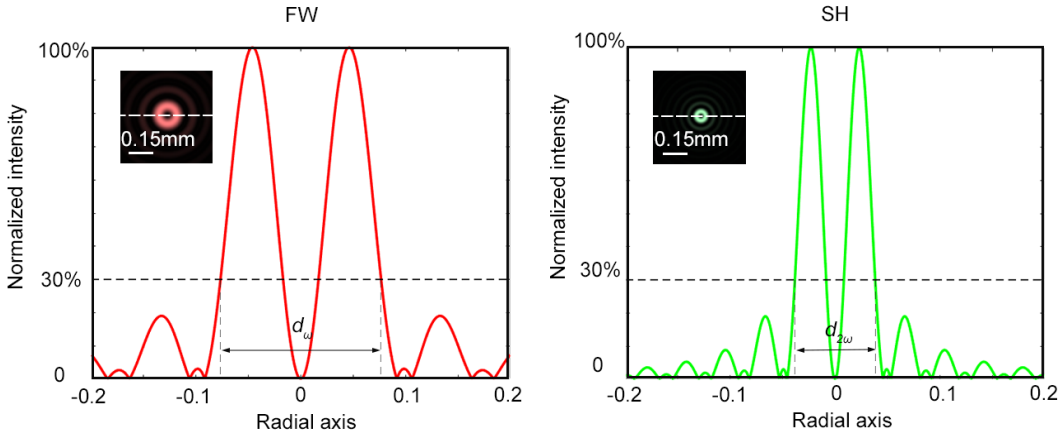

Supplementary Note 3: The relationship between the spatial frequency shift for linear (d_1) and nonlinear (d_2) Raman-Nath diffraction processes

In k-space, the reciprocal vector provided by the OAM-preserved hologram can be expressed as G. The linear and nonlinear Raman-Nath diffraction configurations are shown in the figure below.

For FW, when the diffraction angle θ_1 in the linear Raman-Nath is small, the spatial frequency shift (d_1) can be expressed as

$$d_1 \approx \frac{G\lambda f}{2\pi} \tag{S8}$$

Here, f is the focal length of the Fourier lens.

As for SHW, due to the Snell's law of refraction, the spatial frequency shift (d_2) can be expressed as

$$d_2 \approx \frac{G\lambda f}{4\pi} \tag{S9}$$

As a result, the relationship of d_1 and d_2 is

$$d_1 \approx 2d_2 \tag{S10}$$

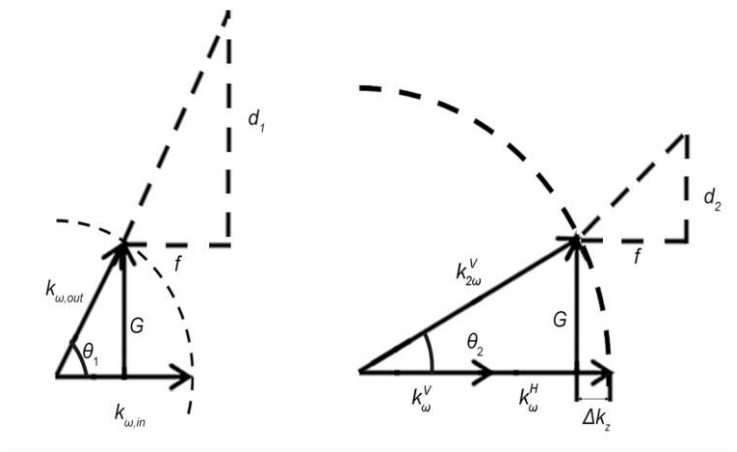

Supplementary Note 4: The intensity distribution of SH images reconstructed from OAM-preserved hologram with uniform Fourier coefficient

According to Fig. 2c, the sampling distance d of $l_\omega^V = 4$ is used for the calculation in this part. When the Fourier coefficient of the OAM-preserved hologram is uniform, the FW image reconstructed in the Fourier plane is an array (for example, 10*10 in the left panel of Fig. 2d) of Gaussian spots with the same intensity. Therefore, the OAM-preserved hologram can be divided into 100 reciprocal vectors ($G_{M,N}$) in k-space (M, N =-4, -3, -2…5) with the same Fourier coefficients. $G_{M,N}$ can be expressed as

$$G_{M,N} \approx \sqrt{M^2 + N^2}\,\frac{2\pi d}{\lambda_\omega f} \tag{S11}$$

As shown in Fig. 2b, the phase-mismatch induced by $G_{M,N}$ can be expressed as

$$\Delta k_{M,N} = k_{2\omega}^V - \sqrt{(k_{2\omega}^V)^2 - (G_{M,N})^2} \tag{S12}$$

Based on the the expression of SH conversion efficiency in nonlinear Raman-Nath diffraction $\eta \propto \left\{ \sin c\left[z\left(\Delta k_{M.N} - \frac{G^2}{2k_{2\omega}} \right) / 2 \right] \right\}^2$, the intensity distribution of SH images in the Fourier space can be calculated (right panel of Fig. 2d).

Supplementary Note 5: The effect of using phase-only hologram rather than complex amplitude hologram

Consider a complex amplitude hologram H_1 that consists of two phase-only holograms of $\exp(i\alpha)$ and $\exp(i\beta)$, i.e.,

$$H_1 = \exp(i\psi_1) + \exp(il_{en}\varphi)\exp(i\psi_2) = \exp(i\alpha) + \exp(i\beta) \tag{S13}$$

When the maximum amplitude modulus of H_1 is normalized, it can be expressed as

$$H_1 = \cos(\frac{\alpha-\beta}{2})\exp[\frac{i(\alpha+\beta)}{2}] \tag{S14}$$

In our experiment, the amplitude part of H_1 is ignored, the phase-only NOMH (H_1) can be expressed as

$$\begin{aligned} H_1 &= \mathrm{sgn}[\cos(\frac{\alpha-\beta}{2})]\exp[\frac{i(\alpha+\beta)}{2}] \\ &= \frac{4}{\pi}[\cos(\frac{\alpha-\beta}{2}) - \frac{1}{3}\cos(\frac{3(\alpha-\beta)}{2}) + \frac{1}{5}\cos(\frac{5(\alpha-\beta)}{2}) - \cdots]\exp[\frac{i(\alpha+\beta)}{2}] \end{aligned} \tag{S15}$$

Considering that the effective value of a cosine function is $1/\sqrt{2}$, the average energy of a general complex electrical field H_1 is 1/2. Taking into account $\sum \frac{1}{n^2} = \frac{\pi^2}{8}$ (n=1,3,5…), the average energy of the phase-only electrical field H_1 is 1. Therefore, under the same pump conditions, the SHG conversion efficiency of the phase-only hologram is twice as that of complex amplitude hologram.

After comparing Eq. (S14) with Eq. (S15), one can find that the phase-only hologram H_1 can be rewritten as

$$H_1 = \frac{4}{\pi}[\cos(\frac{\alpha-\beta}{2}) - \frac{1}{3}\cos(\frac{3(\alpha-\beta)}{2}) + \frac{1}{5}\cos(\frac{5(\alpha-\beta)}{2}) - \cdots]\exp[\frac{i(\alpha+\beta)}{2}]$$
$$= \frac{4}{\pi}H_1 + \frac{4}{\pi}[-\frac{1}{3}\cos(\frac{3(\alpha-\beta)}{2}) + \frac{1}{5}\cos(\frac{5(\alpha-\beta)}{2}) - \cdots]\exp[\frac{i(\alpha+\beta)}{2}] \quad \text{(S16)}$$

Except for the first term, the rest terms appear due to the lack of the amplitude part of H_1, leading to a negative effect on the reconstructed image.

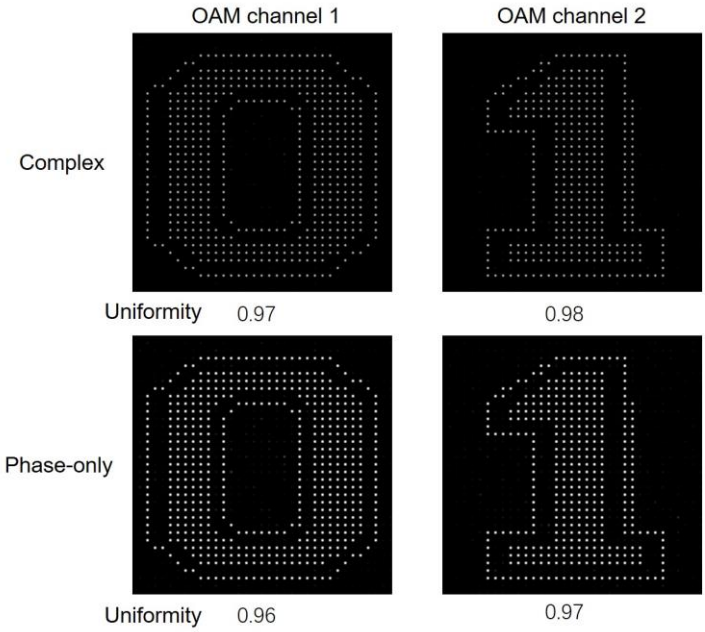

However, the decrease in the image quality is not substantial. As shown in the figure above, two patterns are encoded into two separate OAM channels, and the reconstructed images by using complex-amplitude and phase-only holograms are compared. The uniformity (i.e., the evaluation parameter to define the difference between the reconstructive image and the origincal image [40]) are almost the same for these two kinds of holograms. When the uniformity is 1, the reconstructive image is exactly the original one.

Supplementary Note 6: A proposed experimental scheme of a cascaded type-II third harmonic generation process

A cascaded type-II third harmonic generation can be realized in the subsequent scheme. The OAM-multiplexing hologram is loaded on a horizontally polarized fundamental wave, and a decoding OAM is loaded on a vertically polarized fundamental wave. Both

the hologram and the decoding OAM are imaged into the optical nonlinear system. The optical nonlinear system is chosen to satisfy the phase matching condition for a type-II cascade third harmonic generation.

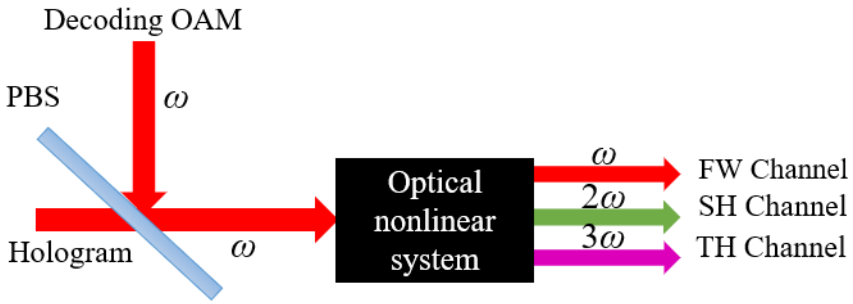

The first step is similar to the process in Fig. 3 of the main text; the horizontally polarized fundamental wave carrying the OAM-multiplexing hologram interacts with the vertically polarized decoding fundamental wave, which results in the designed patterns in fundamental wave and second harmonic wave. Next, the generated second harmonic wave interacts with the vertically polarized decoding fundamental wave, which forms the pattern in the third harmonic (TH) channel. Supplementary Figure 8 presents the simulated results.

Such optical nonlinear system to realize cascade third harmonic generation has been realized in several configurations [34, 41]. By cascading higher-order harmonic generation processes, OAM-multiplexing nonlinear holography can be easily extended to more optical frequency channels.

Supplementary Note 7: The relationship between the resolution of holographic images and the pixel size of OAM-preserved holograms

The maximum diffraction angle of a digital phase hologram can be expressed as $\theta_{\max} = \tan^{-1}(\lambda/2p)$,where λ is the wavelength of FW and p is the single pixel size of a hologram. As such, the maximum size of a reconstructed image is given as $D_{\max} = 2f * \tan\theta_{\max}$, where f is the focal length of the Fourier lens. For OAM-preserved hologram designed for an incident OAM beam with a topological charge of l, the sampling distance d can be achieved according to Supplementary note 2. Thus, resolution of the holographic image ($M * M$) can be calculated by $M = D_{\max}/d$. Our simulation results in Supplementary Fig. 9 shows that the holographic image

resolution can be improved by decreasing the pixel size of the hologram.

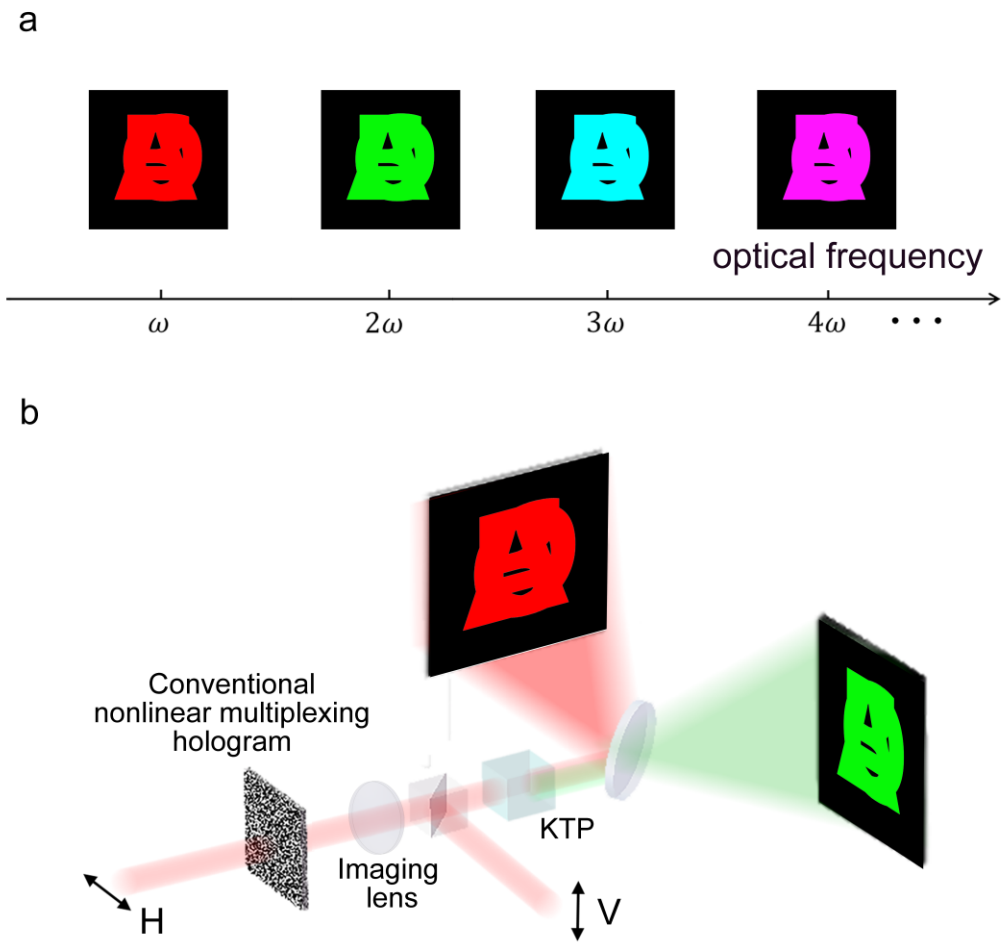

Supplementary Fig. 1. The dilemma in conventional nonlinear multiplexing holography. (a) Nonlinear interacting fields are coupled to each other, which lead to severe inconvenience in simultaneously utilizing different optical frequency components. (b) The conventional high-dimensional nonlinear multiplexing hologram cannot distinguish multiple patterns in the FW and SHW channels.

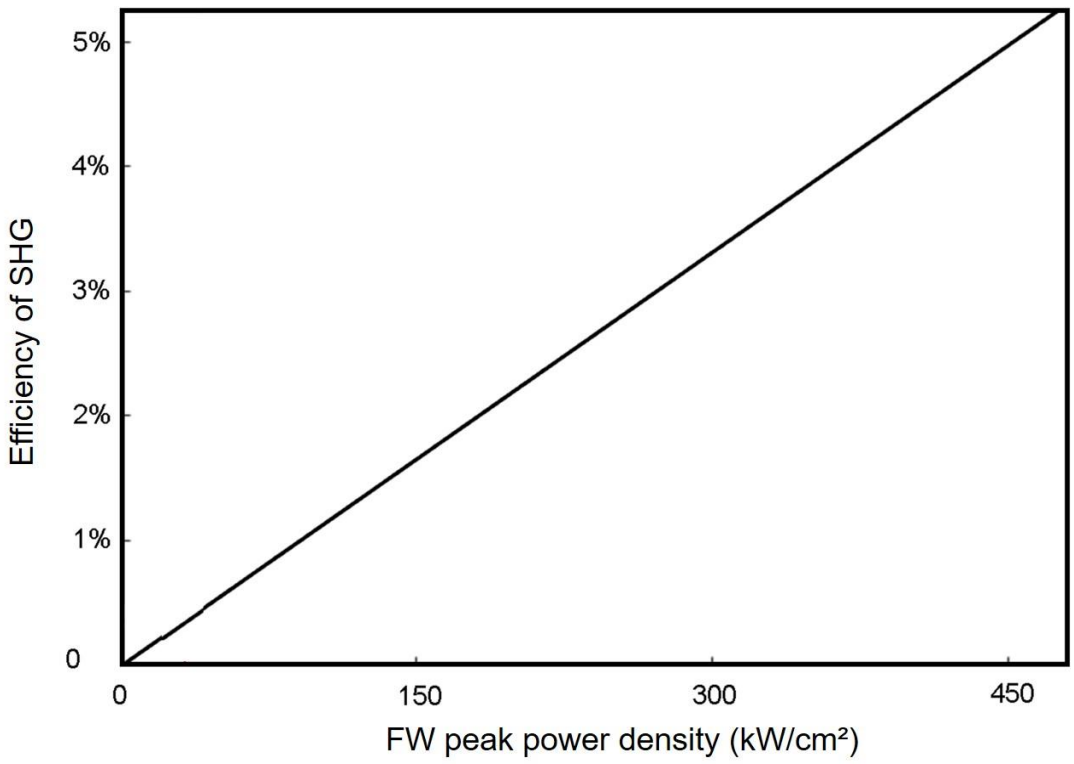

Supplementary Fig. 2. Theoretical relationship of SHG efficiency and input FW peak power density in a phase-matching type-II KTP crystal.

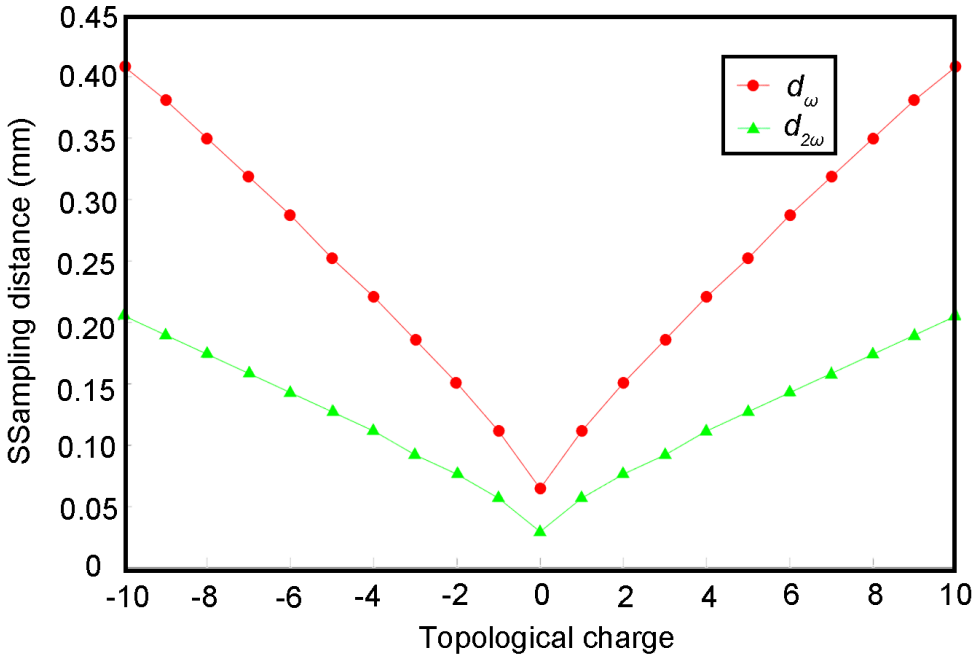

Supplementary Figure 3. Sampling distance constant of FW (d_ω) and SHW ($d_{2\omega}$) in OAM holography.

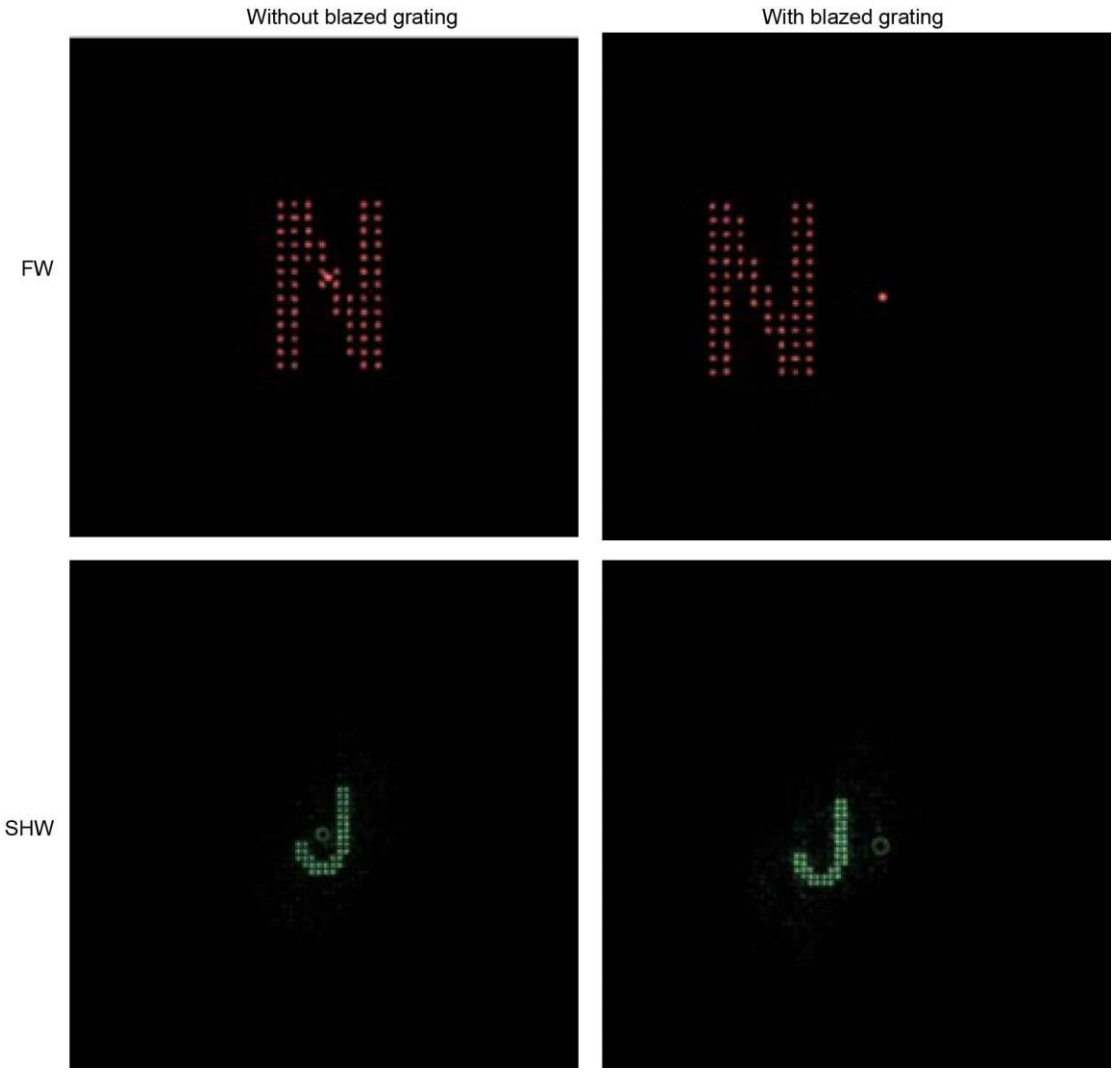

Supplementary Figure 4. Modelled FW and SHW images reconstructed from NOMH with and without blazed grating.

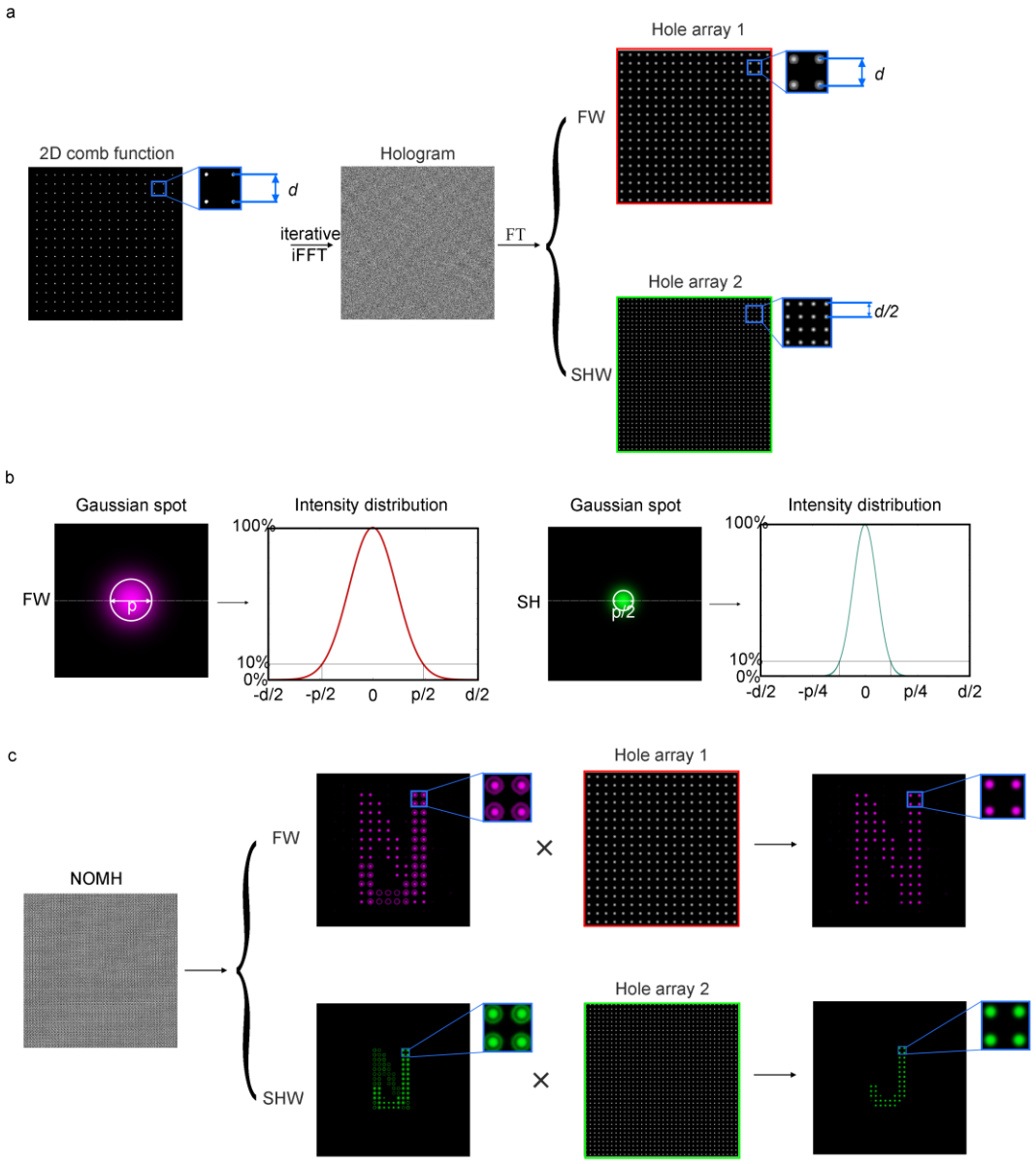

Supplementary Figure 5. Design and effect of the hole array (simulation results). (a) A hologram is designed to define the position and period of the hole array. (b) Determination of the size of a single hole. As a pixel of the reconstructive Gaussian spot array, the area featuring an intensity of more than 10% of its maximum is defined as the effective area of a single hole. (c) In order to further improve the SNR, hole arrays are multiplied on the FW and SHW reconstructive images in Figure 3.

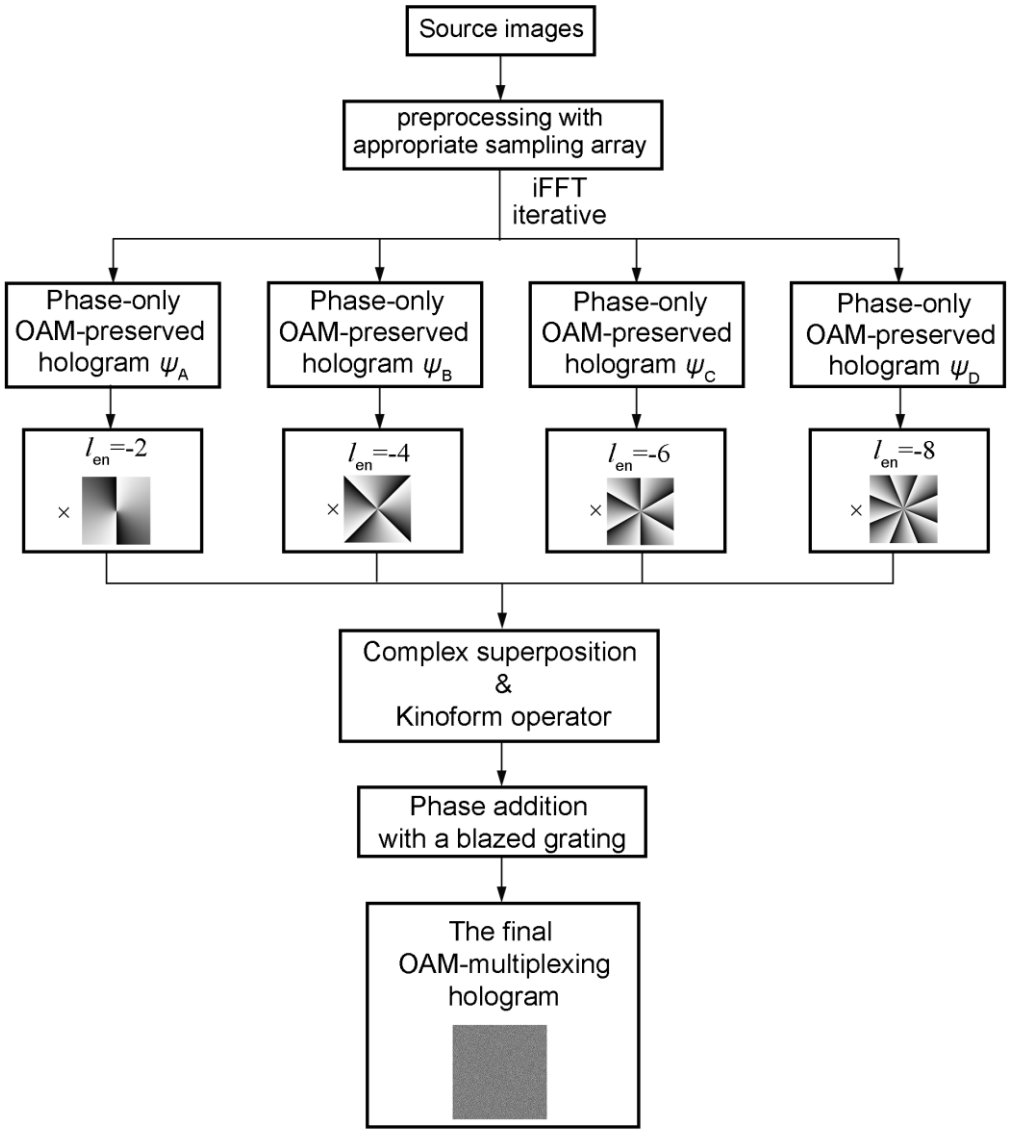

Supplementary Figure 6. Flowchart of the NOMH design in Figure 4.

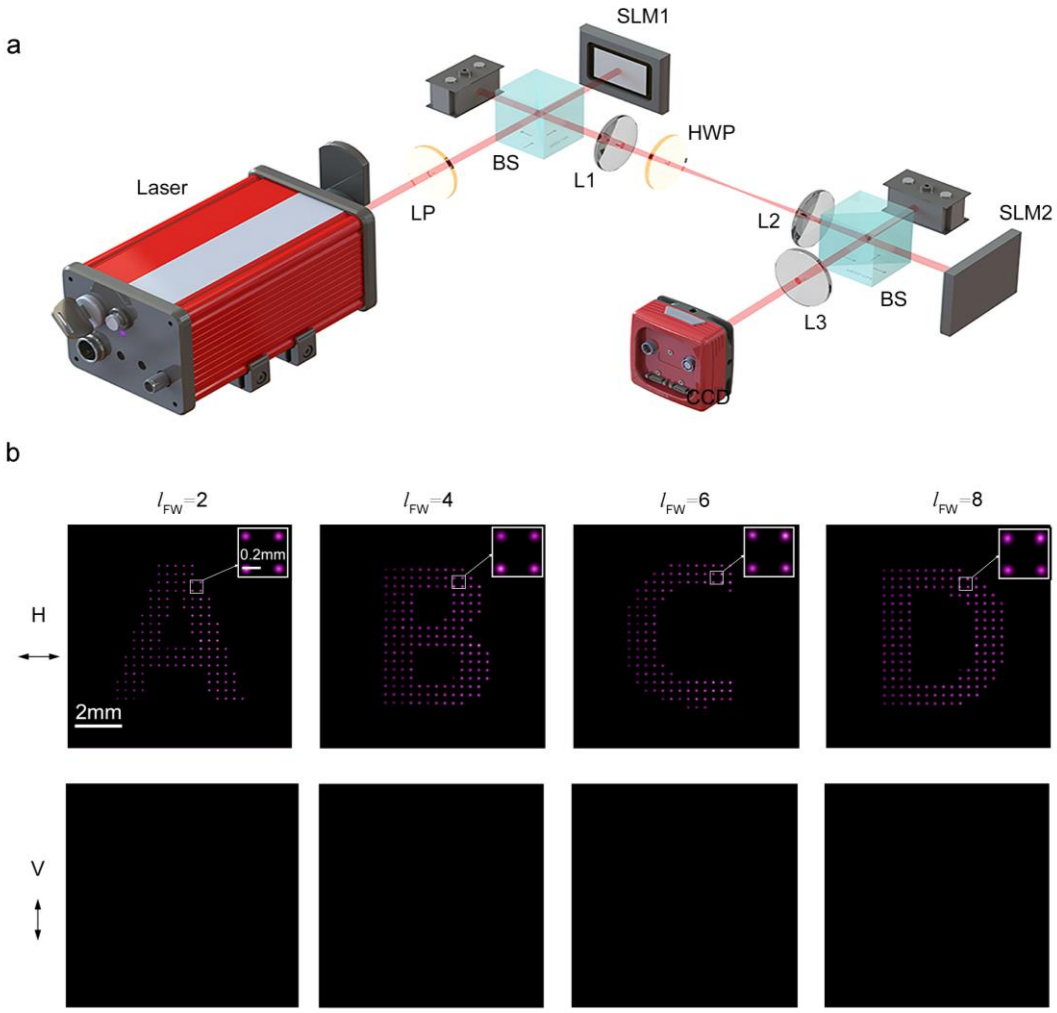

Supplementary Figure 7. Multiple FW images reconstruction from NOMH (experimental data). **a**. The schematic of the experimental setup for FW OAM-multiplexing multi-channel holography. **b**. The images (top) in the FW channel are reconstructed by horizontally-polarized fundamental OAM beams of l_{de}=2, 4, 6, 8, respectively. The FW channel is switched off when using a vertically polarized FW (bottom).

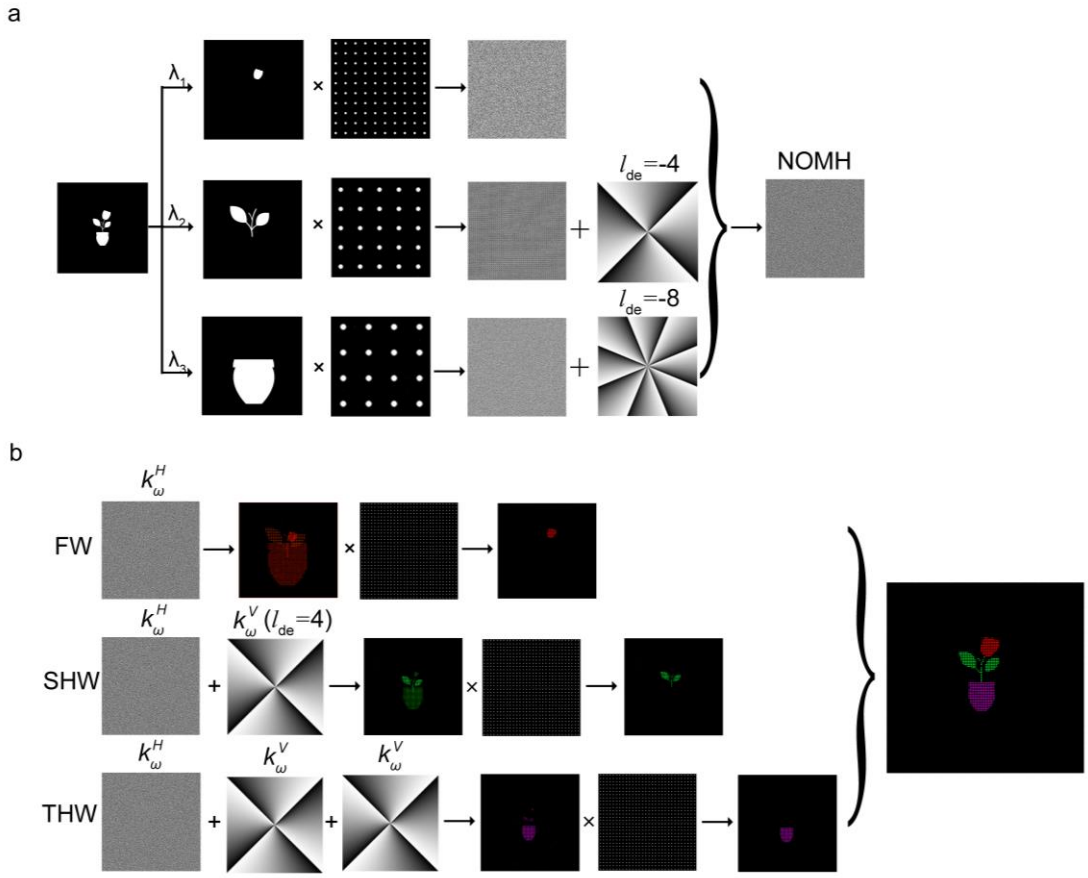

Supplementary Figure 8. OMNH in a cascaded type-II third harmonic generation (simulation results). (a) Design of NOMH for cascaded third harmonic generation processes. (b) Simulation results of three distinctive images reconstructed simultaneously in the FW, SHW, and THW wavelength channels by a decoding OAM beam (l_{de}=4) with a vertical polarization.

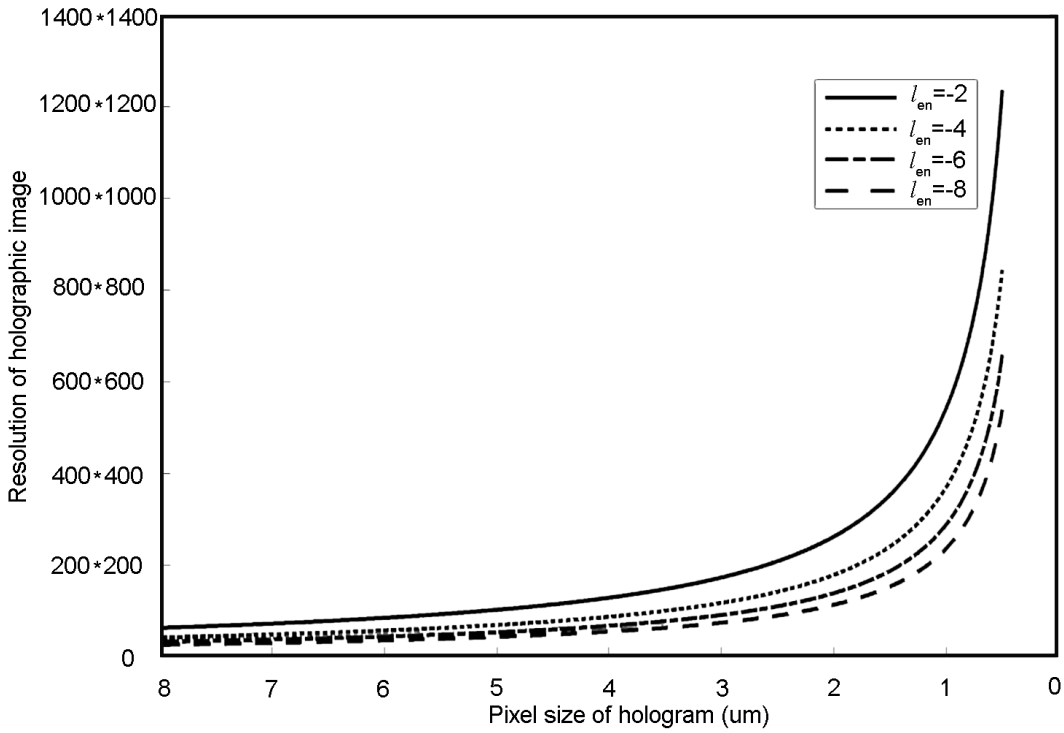

Supplementary Figure 9. Theoretical calculation of the resolution of holographic image as a function of pixel size of the hologram.

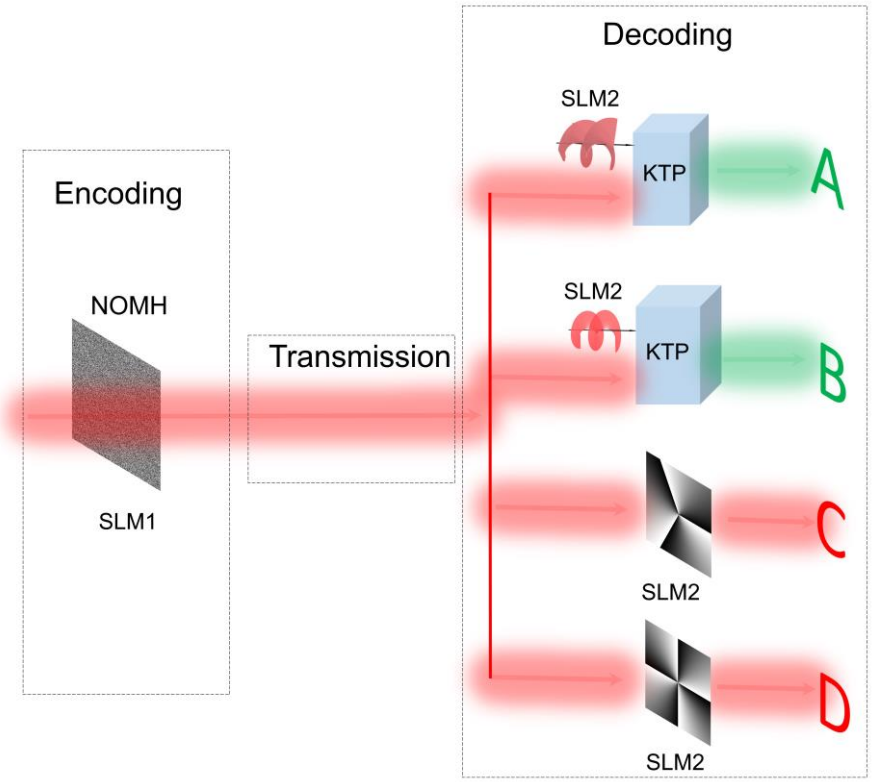

Supplementary Figure 10. Proposed scheme for dual-wavelength multicasting in optical communications. Based on MCNH, the encoding hologram (imprinted by SLM1) is carried by the infrared light, which includes the information of both FW and SHG. In the decoding processes, the spiral phases are loaded on SLM2, and customers can use the experimental setups in Figure 3 and supplementary Figure 7 to achieve the SHG (Letter A and Letter B) and FW information (Letter C and Letter D), leading to dual-wavelength channel multicasting.